Suspension-to-Surface Heat Transfer in a Circulating-Fluidized-Bed Combustor

Heat transfer coefficients were measured for circulating beds of sand particles of mean size 222 to 299 μm at temperatures of 340–880°C. Transfer coefficients were obtained for both a 1.22-m-long, 12.7-mm-OD vertical tube and a 1.59-m-long, 148-mm-wide membrane wall near the top of a 152-mm-square by 7.32-m-tall combustion column. For both surfaces and all temperatures, average heat transfer coefficients increased almost linearly with local suspension density which ranged from 0 to 70 kg/m^3. Radiation played a significant role, especially at high temperatures and low suspension densities. Heat transfer coefficients also varied significantly with the lateral position of the tube. The vertical length of heat transfer surface is shown to be an important parameter allowing seemingly discrepant published results to be reconciled.

Richard L. Wu
John R. Grace
C. Jim Lim
Clive M.H. Brereton
Department of Chemical Engineering
and Pulp and Paper Center
University of British Columbia
Vancouver, Canada V6T 1W5

Introduction

While circulating fluidized beds continue to gain wide acceptance, especially for gas-solid reactions like calcination and combustion, there are still many fundamental areas which are little understood. Research in heat transfer in circulating beds, for instance, remains largely empirical with few published results available for public dissemination (Grace, 1986; Glicksman, 1988). Theoretical modeling attempts are hindered by the fact that these published data are extremely scattered when compared against one another.

In this paper, we present experimental data for sand particles of 222 to 299 μm obtained from a tube and a membrane wall at temperatures of 340–880°C. The effect of lateral position of the tube is also investigated. Analyses of local heat transfer coefficient profiles along the membrane wall are then presented to demonstrate the significant influence of the vertical length of heat transfer surface.

Experimental Equipment

All the experimental data in this paper were obtained using the circulating-fluidized-bed combustion (CFBC) facility at the University of British Columbia. Many details of the equipment are provided in previous papers (Wu et al., 1987; Grace et al., 1987; Legros et al., 1989). Only a brief description of the key details relevant to the heat transfer results are provided here.

A schematic of the major experimental components is shown in Figure 1. The refractory-lined reactor column is 7.32-m-high and 152 × 152 mm in cross section. For the studies with the membrane transfer surface, the bottom section of the reactor column was a refractory-lined stainless-steel section with its inside tapered from a 51 × 152 mm cross section to 152 × 152 mm cross section over its 1.22-m height to provide a high acceleration zone, reducing sintering and agglomeration. The entire riser is instrumented with thermocouples and pressure taps at 0.61 m intervals along opposite walls for the determination of temperature and density profiles. For the tapered bottom section, primary air was introduced through a horizontal half-pipe cut along its axis to form a distributor with twenty 9.5-mm-diameter orifices drilled on its curved surface. For the experiments with the vertical cooling tube, the distributor had three tuyeres each with six inclined holes. Preheated secondary air was introduced through two pairs of directly opposed air ports 0.9 m above the distributor. Solids entrained in the column were continuously captured by a 0.31-m-ID refractory-lined primary cyclone and returned 0.4 m above the bottom of the column via an L-valve. The solids recirculation rate was controlled by varying the flow of aeration air to the L-valve. Fines not captured by the primary cyclone were captured with a 0.2-m-ID secondary cyclone and could be returned to the bottom of the reactor via an eductor.

The first set of heat transfer data was obtained from a 1.22-m-long, 12.7-mm-OD water-cooled stainless-steel tube beginning 4.57 m above the distributor on one wall of the column. This tube was normally positioned touching the refractory surface midway between two faces of the column. It could also be moved to the axis of the column or intermediate lateral posi-

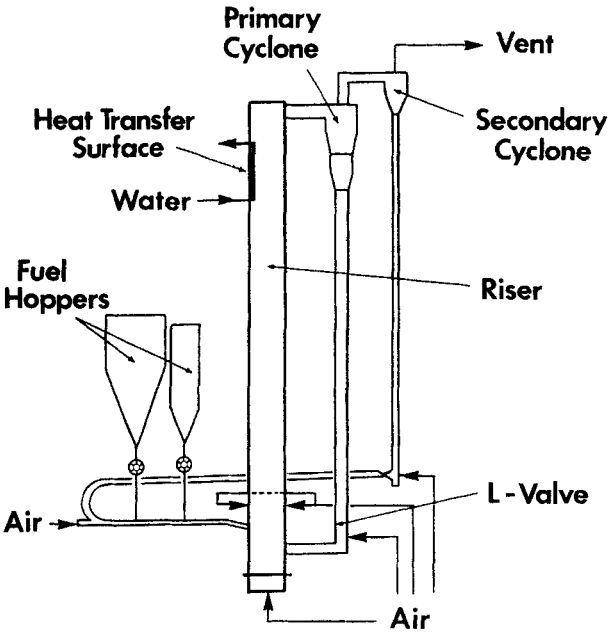

Figure 1. Circulating-fluidized-bed combustion facility.

tions. Both the inlet and outlet temperatures as well as the flow rates of the cooling water were recorded, allowing the total heat flux to be calculated.

In the second set of experiments, a 1.59-m-long by 148-mm-wide water-cooled membrane wall was used as the heat transfer surface, beginning 4.27 m above the distributor on one wall of the column. This surface consisted of four identical, half-embedded, vertical, schedule-80 stainless-steel tubes connected longitudinally by flat fins to form a membrane wall. (See Figure 2.) The fins were flush with the refractory surface above and below. One of the central tubes was instrumented with ten thermocouples approximately 150 mm apart. Both the temperatures and flow rates of the water inside the tube were recorded.

Although the predominant heat transfer resistance for the present conditions is on the circulating bed side of the heat transfer surface, results reported in this paper are suspension-to-exposed-surface values, where the water-side resistance, estimated from Sleicher and Rouse (1975), and the tube resistance have been subtracted. The membrane wall coefficients are based on the total exposed areas of the tubes and the fins.

The combustion fuel used in the tube heat transfer experiments was Minto coal, premixed with Elmtree limestone. Highvale coal was used as the fuel in the membrane wall experiments. In all the experiments, Olivine sands were used as the inert bed materials. Some relevant physical properties of the sand and limestone are given in Table 1. Typical composition of the bed materials is about 20% sand, 55% limestone, with the remainder ash and char. Detailed particle-size analyses of various runs are given in Table 2. The mean particle sizes are calculated from the inverse of $\Sigma(x_i/d_{pi})$, where x_i is the weight fraction of particles which have an average size of d_{pi} determined by sieve analysis.

Results and Discussion

The variations of average overall heat transfer coefficient with local suspension density are plotted in Figure 3 for the vertical tube at four different suspension temperatures with the tube touching the near wall of the column. As in previous work, suspension densities are cross-sectional average values estimated from the pressure profiles in the riser. In all cases, the

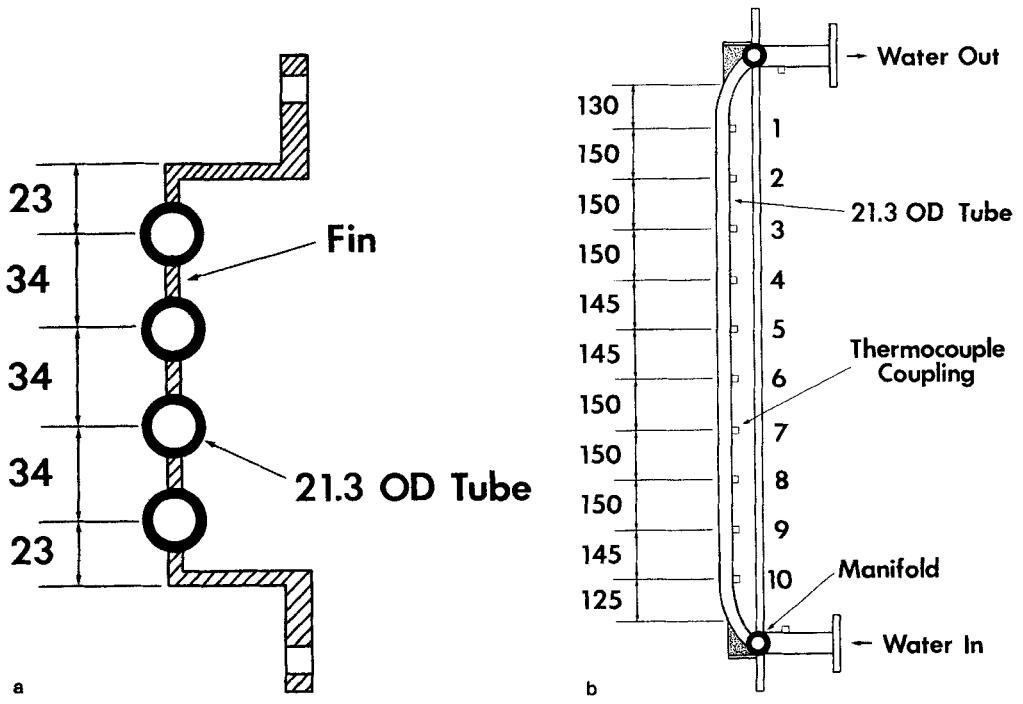

Figure 2. Membrane wall heat transfer surface (in mm).
a. *Plan view*
b. *Section view*

Table 1. Physical Properties of Sand and Sorbent

	Olivine 70 Sand	Elmtree Limestone
Part. Dens., kg/m³	3,066	2,400
Mean Part. Dia., μm	241	210
Voidage at Min. Fluidiz.	0.46	0.44
Min. Fluidiz. Vel. at Room Temp., m/s	0.071	0.043

Table 2. Particle Size Analyses of Different Runs

μm	wt. %				
Size	Run 1	Run 2	Run 3	Run 4	Run 5
1,410+	1.5	0.4	0.2	0.0	0.0
1,410–1,000	0.8	0.8	0.5	0.0	0.0
1,000–707	2.7	4.3	3.3	0.2	0.0
707–500	13.2	10.8	16.0	0.3	0.0
500–354	30.3	20.8	34.7	2.6	5.8
354–250	21.4	24.5	23.3	38.0	48.6
250–177	14.4	18.5	13.7	45.6	36.1
177–125	6.8	10.5	5.0	10.1	6.6
125–88	3.4	5.0	1.7	1.9	1.7
88–53	2.6	2.1	0.7	0.8	1.2
53–44	0.9	0.5	0.2	0.1	0.0
44–0	2.0	1.8	0.7	0.4	0.0
Mean Part. Size, μm	241	227	299	222	241

average heat transfer coefficient increases linearly with suspension density. The lines shown are least-squares best-fit lines. While there are small differences in the superficial gas velocity for the four different symbols and the average particle size for the lowest suspension temperature is slightly larger, the effects of these variables on the average heat transfer coefficient are small for a long heat transfer surface (Wu et al., 1987). Since radiation is small for the lowest suspension temperature of 343°C and the factors which influence the particle- and gas-convective components of heat transfer are not influenced greatly by temperature, the difference between this line and the other lines gives a good estimate of the radiation contribution to the average heat transfer coefficient. The similarity in the slopes for the four lines suggests that radiation is relatively independent of suspension density. The fraction of the total transfer due to radiation, however, varies strongly with the suspension density, radiation being the predominant heat transfer mechanism for dilute (low load) systems at typical combustion temperatures (850–900°C). This compares with bubbling-fluidized-bed combustion systems where radiation typically accounts for only about 20% of the total transfer, even at low loads.

The corresponding variations of average overall heat transfer coefficient with local suspension density for the membrane wall are shown in Figure 4 for three suspension temperatures. Again, the average coefficient increases linearly with suspension density, although the rate of increase is in general not as steep as that for the tube. As in the previous case, the slopes of the best-fit lines in Figure 4 are very similar to each other.

In CFBC studies, as in bubbling-fluidized beds, it is common

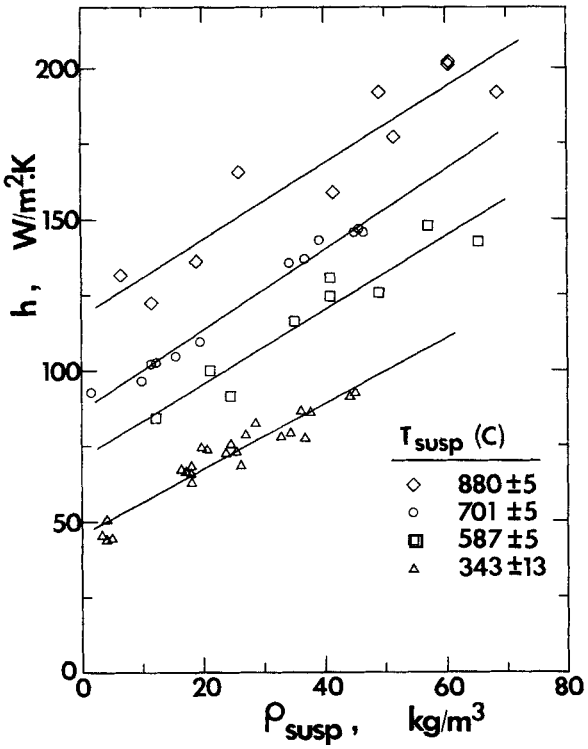

Figure 3. Overall heat transfer coefficient for vertical tube vs. suspension density at different suspension temperatures.

For particle-size distributions, see Table 2. Bottom line: Run 3, U = 6.5 m/s. Other lines: Run 1, U = 6.6–8.6 m/s.

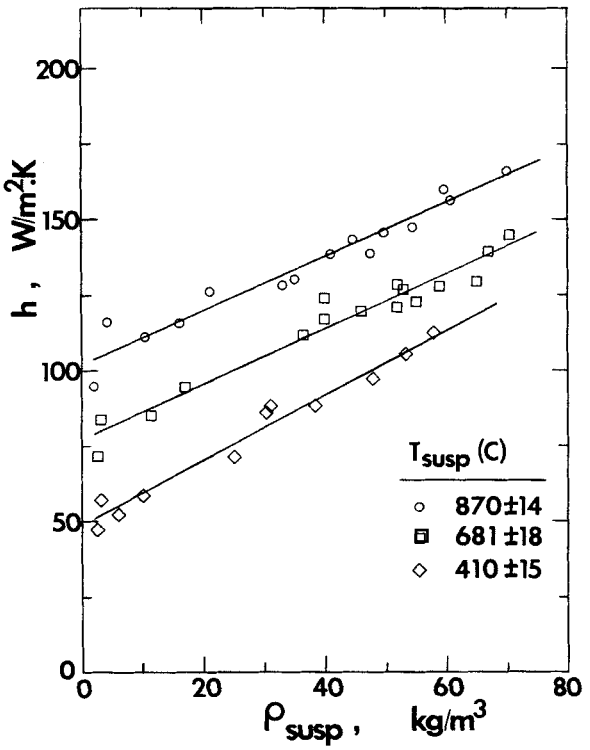

Figure 4. Overall heat transfer coefficient for the membrane wall vs. suspension density at different suspension temperatures.

Bottom line: Run 5 in Table 2, U = 7.5 m/s. Other lines: Run 4 in Table 2, U = 8.8–9.5 m/s.

to assume that the overall heat transfer coefficient can be estimated from

$$h = h_{gc} + h_{pc} + h_{rad} \tag{1}$$

where h_{gc} and h_{pc} are the gas- and particle-convective components, respectively, while h_{rad} is the radiative component. Table 3 shows the comparison of the calculated heat transfer coefficients based on Eq. 1 with the experimental values of the vertical tube from Figure 3. The comparison is made at two suspension densities of 15 and 60 kg/m^3. h_{gc} is estimated from the correlation of Sleicher and Rouse (1975) for an empty column. It is recognized that the gas flow pattern in the presence of solids is different from that in an empty column. Since this component is generally small, however, the estimate from an empty column is sufficient as a first approximation. The radiative component, h_{rad}, is estimated by treating the gas-solids suspension as a gray body such that

$$h_{rad} = \frac{\sigma(T_{susp}^4 - T_{surf}^4)}{(1/\epsilon_{susp} + 1/\epsilon_{surf} - 1)(T_{susp} - T_{surf})} \tag{2}$$

where T_{susp} and T_{surf} are the temperatures of the suspension and the tube surface, respectively. Both the emissivity values, ϵ_{susp} and ϵ_{surf}, are set equal to 0.91 to fit the highest suspension temperature of 880°C. The difference between the best-fit line of the experimental data at 880°C and the sum of h_{gc} and h_{rad} is taken to be h_{pc}, which is assumed to apply also at the lower temperatures. While the various heat transfer mechanisms are not strictly additive (Chen et al., 1988) and the actual radiative exchanges in a combustor are complex, it can be seen from Table 3 that the estimated and experimental overall coefficients obtained at the three lower suspension temperatures show extremely good agreement. This suggests that Eq. 1 provides a useful practical basis for fast fluidized-bed conditions.

Figures 3 and 4 are cross-plotted in Figure 5 to show the variations of the overall time-mean heat transfer coefficient with suspension temperature at four different suspension density levels for both the vertical tube and the membrane wall. It can be seen from Figure 5 that radiation starts to become a significant factor beyond a suspension temperature of about 400°C for both heat transfer surfaces. The relative magnitude of radiation

Table 3. Comparison of Experimental Data with Estimated Heat Transfer Coefficient for the Vertical Tube*

kg/m^3	°C		W/m^2 · K				
Susp. Dens.	Avg. Susp. Temp.	Tube Surf. Temp.	Gas Conv. Comp.	Particle Conv. Comp.	Rad. Comp.	Total Est. h	Exp. Data h
15	701	83	13	19	68	100	106
	587	56	13	19	48	80	89
	343	45	14	19	22	55	62
60	701	83	13	76	68	157	166
	587	56	13	76	48	137	144
	343	45	14	76	22	112	110

*At three lower temperatures based on Eq. 1 with emissivities and particle convective component estimated from the results at 880°C and the gas convective component obtained from the correlation of Sleicher and Rouse (1975).

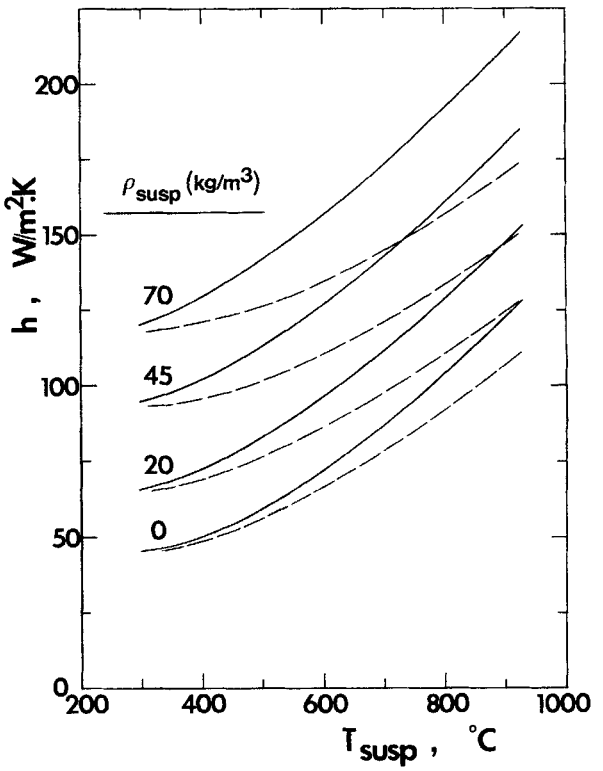

Figure 5. Cross plot of overall heat transfer coefficient vs. suspension temperature for vertical tube (solid lines) and membrane wall (broken lines) at different suspension density levels.

increase, however, is quite different for the two different geometries. The vertical tube has a much larger radiative increase than the membrane wall at the same suspension temperature. This is probably due to the better view factor enjoyed by the tube as compared to the membrane wall where the half-embedded tubes "see" their relatively cool partners to a significant extent. The emissivity of the two surfaces could also be somewhat different. Figure 5 also indicates that the two sets of curves are closer together at suspension temperatures below 400°C. This is expected since the effect of radiation diminishes as the suspension temperature decreases. Residual differences are then no doubt due to the different geometries of the single tube and the membrane surface.

The effect of lateral position of the vertical tube on the average heat transfer coefficient is shown in Figure 6, which plots the variations of heat transfer coefficient with suspension density for four different lateral positions and two suspension temperatures. Although the superficial gas velocities and particle sizes again differed slightly, the effects of these variations on the heat transfer coefficient are small. The difference between the two sets of curves is, therefore, predominantly due to the temperature effect. For the lower temperature of 343°C, the position near the wall always exhibits the highest heat transfer coefficient compared to the other three positions in the range of suspension density investigated (0–60 kg/m^3). The trend, however, is quite different for the higher temperature of 854°C where the center of the column almost always exhibits the highest coefficient. For low suspension density (<20 kg/m^3), the heat transfer coefficient decreases from the center of the column

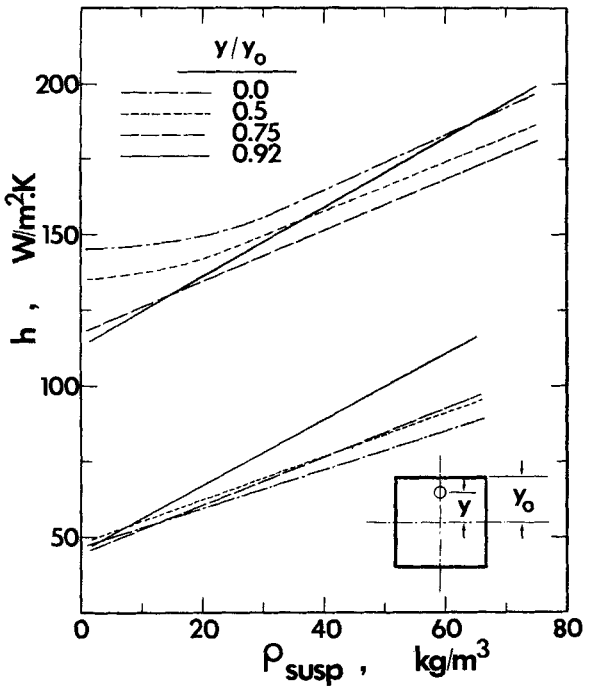

Figure 6. Overall heat transfer coefficient vs. suspension density for different lateral tube positions and suspension temperatures.

Top four curves: Run 2 in Table 2, U = 9.3 m/s, T_{susp} = 854 ± 3°C. Bottom four curves: Run 3 in Table 2, U = 6.5 m/s, T_{susp} = 343 ± 13°C.

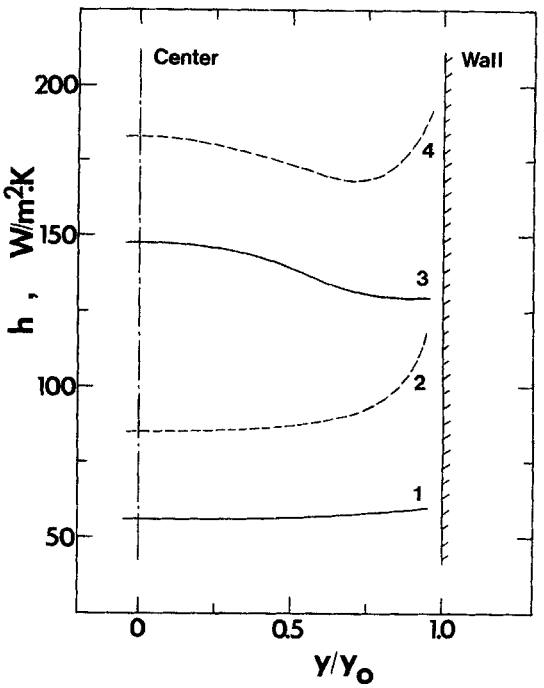

Figure 7. Cross plot of overall heat transfer coefficient vs. lateral tube position for different suspension densities and suspension temperatures.

Solid lines: ρ_{susp} = 15 kg/m³. Broken lines: ρ_{susp} = 60 kg/m³. Curves 1, 2: T_{susp} = 343°C. Curves 3, 4: T_{susp} = 854°C.

to a minimum near the wall. For higher suspension density (>30 kg/m³), the heat transfer coefficient decreases as the tube moves from the center towards the wall of the column before increasing again when the tube is immediately adjacent to the wall.

The influence of the lateral position is better illustrated in Figure 7 which is a cross plot of Figure 6 plotting the heat transfer coefficient vs. the lateral position of the vertical tube at two suspension density levels. For the lower temperature of 343°C where the effect of radiation is small, particles are relatively evenly dispersed at low suspension densities. This is reflected in the similar heat transfer coefficients across the cross section of the column for the suspension density of 15 kg/m³. As the suspension density increases, the wall region of the bed displays the highest particle convective heat transfer coefficient due to the development of a denser wall region, in which particles tend to congregate and move downward along the wall. On the other hand, for the higher temperature of 854°C where radiation has a significant effect, the relative lateral position of the vertical tube plays a more important role due to the shielding effect. As the tube is moved from the center of the column where it can "see" all four hot walls to a position next to a partially-cooled wall, the radiative heat transfer decreases. This explains the increase in the heat transfer coefficient at low suspension density as the tube is moved from the wall to the center of the column. With an increase in suspension density and the development of a denser wall region, the heat transfer coefficient near the wall also increases. It is interesting to note that the more complicated curve 4 in Figure 4 can be obtained by superimposing the difference between curves 1 and 2 with curve 3. This again indicates that it is reasonable to treat the various terms in Eq. 1 separately and additively.

In addition to the overall heat transfer coefficients, local heat transfer coefficients along the membrane wall were also obtained for two suspension temperatures. The profiles are plotted in Figure 8 where Z is the position along the membrane wall measured from its top downwards. Similar to the trend reported earlier (Wu et al., 1987), the local heat transfer coefficient decreases with the increase in Z, suggesting a predominantly downflowing wall layer next to the membrane wall surface, with fresh hot sol-

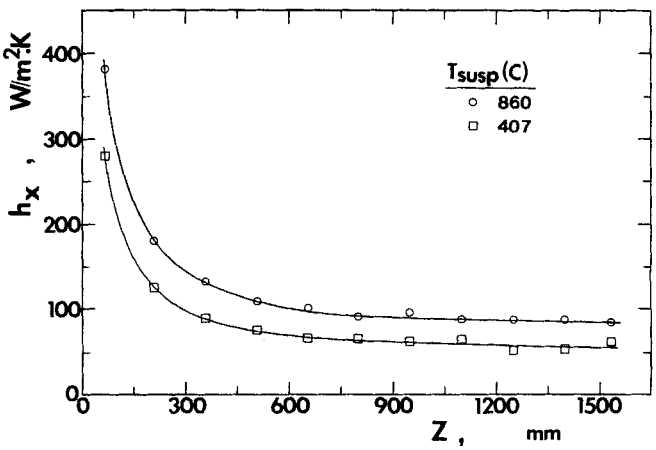

Figure 8. Local heat transfer coefficient along membrane wall vs. Z for different suspension temperatures.

ρ_{susp} = 54 kg/m³, Run 5 in Table 2.

ids coming into contact with the top part of the surface. The slopes for both profiles, if plotted on a log-log scale, are very close to −0.5 suggesting that there is little renewal in this wall layer of particles. As the two curves are obtained for the same suspension density, their differences are predominantly due to the effect of temperature. The larger differences near the top of the surface compared to the bottom are probably due to some cooling of the wall layer particles as they traverse the membrane wall surface, thus reducing the radiation transfer to the surface.

There is a growing consensus (e.g., Hartge et al., 1986; Bader et al., 1988; Rhodes et al., 1988) that solid particles in circulating fluidized beds tend to move upward in a dilute central core, while many then move downward in a denser wall layer. The tendency for solid particles to stay in the downflowing wall layer makes the vertical length of heat transfer surface at the wall one of the critical parameters in any heat transfer study. This is illustrated in Figure 9, where h_Z, defined as the heat transfer coefficient averaged over vertical length Z starting from the top of the membrane wall, is plotted against Z for both suspension temperatures. In both cases, h_Z drops rapidly with Z, much as for laminar flow over a flat plate. As the layer of particles sweeps down along the heat transfer surface, it gradually approaches thermal equilibrium with the surface since there is little renewal in this layer. This reduces the driving force for heat transfer, thus producing a much lower transfer coefficient. It is clear from Figure 9 that, depending on the vertical length of the heat transfer surface, one will obtain very different average heat transfer coefficients which can differ by up to 200%. This helps to explain earlier, seemingly discrepant, published results as discussed later. In general, high heat transfer coefficients are obtained by using very short heat transfer surfaces. As the length of heat transfer surface increases (e.g., over 1 m), there is less influence on the heat transfer coefficient.

Figure 10 shows some previously published heat transfer results for circulating fluidized beds together with the present ones. The results may be grouped into three relatively narrow ranges of mean particle sizes: 87–95 μm, 170–188 μm, and 227–250 μm. In each case, sand particles were employed, and all reported results fall within the suspension density range of 0–100 kg/m^3. Some relevant experimental details of these published studies are summarized in Table 4. Reported heat transfer coefficients in Figure 10 are cross-plotted in Figure 11 against b, the vertical length of heat transfer surface, at a typical circulating bed suspension density of 50 kg/m^3. In spite of the different experimental equipment and operating conditions used in these studies, Figure 11 clearly demonstrates the strong influence of heat transfer surface length, much in the same manner as shown in Figure 9. In addition, it can be seen from Figure 11 that the influence of mean particle size diminishes with longer heat transfer surface. For longer surfaces, the particle residence times on the surface become much larger than the thermal time constants for both large and small particles. This,

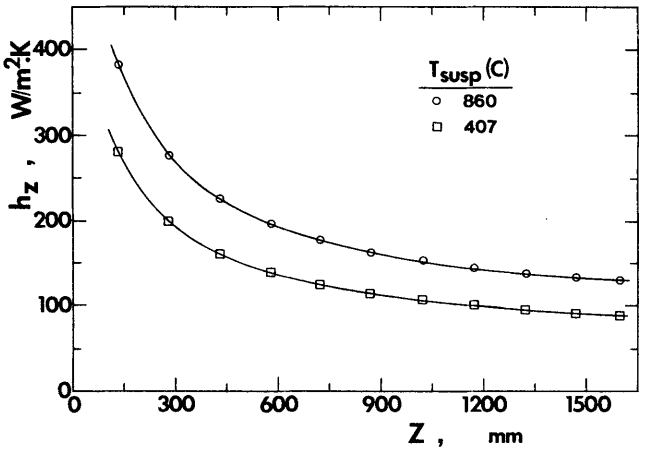

Figure 9. Heat transfer coefficient averaged over Z vs. Z for different suspension temperatures.
ρ_{susp} = 54 kg/m^3, Run 5 in Table 2.

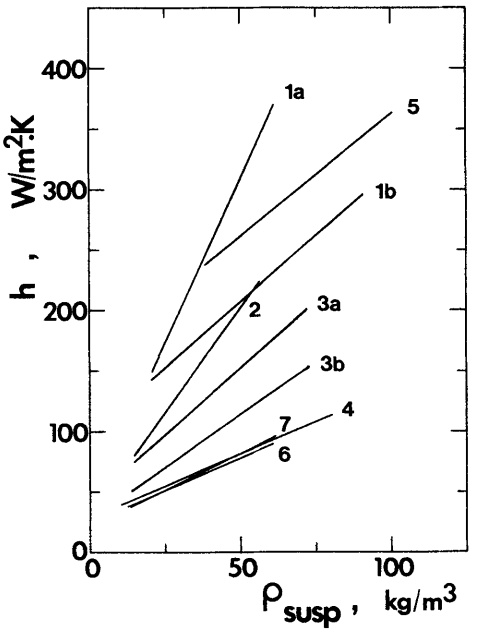

Figure 10. Comparison of published heat transfer results.
For experimental details, see Table 4.

Table 4. Experimental Studies on Heat Transfer in Circulating Fluidized Bed

Curve	Author	Mean Part. Size μm	Avg. Susp. Temp. °C	Vert. Length Heat Transf. Surface mm
1a	Basu and Nag (1987)	87	35	25
1b	" " "	227	38	25
2	Feugier et al. (1987)*	95	400	950
3a	Kobro and Brereton (1986)	170	25	100
3b	" " "	250	25	100
4	Wu et al. (1987)**	188	277	1,530
5	Wu et al. (1989)	171	35	22
	This Work:†			
6	Membrane Wall	241	410	1,590
7	Tube	241	880	1,220

*Since only the particle convective heat transfer coefficient has been reported, the gas convective coefficient estimated from Sleicher and Rouse (1975) has been added. The heat transfer surface length, not given in the paper, is obtained from Glicksman (1988).

**The overall heat transfer coefficients were calculated for inlet and outlet water temperatures instead of those from thermocouple 1–8. Effect of the higher suspension temperature was estimated from Eq. 2.

†Effect of higher suspension temperature was estimated from Eq. 2.

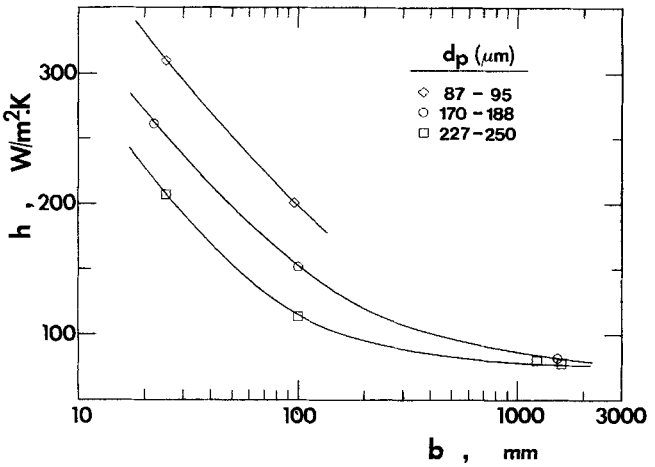

Figure 11. Cross plot of average heat transfer coefficient vs. vertical transfer surface length for different mean particle sizes.

$\rho_{susp} = 50$ kg/m^3.

however, is not true for shorter surfaces where the size of particles becomes a significant factor, with the smallest particles exhibiting the highest particle convective heat transfer coefficient and hence the highest overall coefficients at low temperatures (Grace, 1986). The results and conclusions presented in this paper, coupled with results summarized in the literature (Grace, 1986; Glicksman, 1988) and recent experimental local instantaneous heat transfer measurements (Wu et al., 1989), provide a basis for modeling the heat transfer process in risers operating in the fast fluidized-bed regime. This will be the subject of a future paper.

Conclusions

Overall and local heat transfer coefficients were obtained in a circulating-fluidized-bed combustor at temperatures of 340–880°C for two different heat transfer surfaces: a vertical tube and a membrane wall. Although overall coefficients of both surfaces show linear increases with suspension density at all temperatures, results from the tube are higher than those from the membrane wall, due primarily to higher radiative transfer. Lateral position also influences the overall coefficient significantly for the tube, with higher coefficients near the wall at low temperatures, where the particle convective component is dominant, and at the axis of the column at high temperatures, where radiation plays a strong role. The vertical length of heat transfer surface is found to significantly affect the average heat transfer coefficient. This factor helps to reconcile earlier apparently discrepant results and accounts for the fact that particle size plays a much stronger role for small heat transfer surfaces than for longer ones.

Acknowledgment

We are grateful to Energy, Mines and Resources Canada for providing financial assistance and to the Pulp and Paper Research Institute of Canada for a scholarship to RLW. Assistance of R. Legros, H. Ackroyd, H. Li, J. Zhao, and R. Senior with the experiments is also gratefully acknowledged.

Notation

b = vertical length of heat transfer surface, mm
d_p = surface-volume mean particle size, μm
h = overall time-average heat transfer coefficient, W/m^2 · K
h_{gc} = gas convective component of h, W/m^2 · K
h_{pc} = particle convective component of h, W/m^2 · K
h_{rad} = radiative component of h, W/m^2 · K
h_x = local heat transfer coefficient, W/m^2 · K
h_Z = heat transfer coefficient averaged over the length of transfer surface from $Z = 0$ to $Z = Z$, W/m^2 · K
T_{surf} = heat transfer surface temperature, °C
T_{susp} = suspension temperature, °C
U = superficial gas velocity, m/s
y = distance from tube axis to axis of column, mm
y_o = half width of reactor column, mm
Z = position along membrane wall measured from its top downward, mm

Greek letters

ϵ_{surf} = emissivity of heat transfer surface
ϵ_{susp} = emissivity of suspension
ρ_{susp} = suspension density at a given level averaged over column cross section, kg/m^3
σ = Stefan-Boltzmann constant, 5.672×10^{-8} W/m^2 · K^4

Literature Cited

Bader, R., J. Findlay, and T. M. Knowlton, "Gas/Solids Flow Patterns in a 30.5-cm-diameter Circulating Fluidized Bed," *Circulating Fluidized Bed Technology: II*, P. Basu and J. F. Large, eds., Pergamon, Toronto, 123 (1988).

Basu, P., and P. K. Nag, "An Investigation into Heat Transfer in Circulating Fluidized Beds," *Int. J. Heat Mass Transf.*, **30**, 2399 (1987).

Chen, J. C., S. S. Dou, and R. J. Cimini, "A Theoretical Model for Simultaneous Convective and Radiative Heat Transfer in Circulating Fluidized Beds," *Circulating Fluidized Bed Technology: II*, P. Basu and J. F. Large, eds., Pergamon, Toronto, 255 (1988).

Feugier, A., C. Gaulier, and G. Martin, "Some Aspects of Hydrodynamics, Heat Transfer and Gas Combustion in Circulating Fluidized Beds," *Proc. Int. Conf. on Fluidized Bed Combustion*, 613 (1987).

Glicksman, L. R., "Circulating Fluidized Bed Heat Transfer," *Circulating Fluidized Bed Technology: II*, P. Basu and J. F. Large, eds., Pergamon, Toronto, 13 (1988).

Grace, J. R., "Heat Transfer in Circulating Fluidized Beds," *Circulating Fluidized Bed Technology*, P. Basu, ed., Pergamon, Toronto, 63 (1986).

Grace, J. R., C. J. Lim, C. M. H. Brereton, and J. Chaouki, "Circulating Fluidized Bed Reactor Design and Operation," *Sadhana*, **10**, 35 (1987).

Hartge, E. U., Y. Li, and J. Werther, "Analysis of the Local Structure of the Two Phase Flow in a Fast Fluidized Bed," *Circulating Fluidized Bed Technology*, P. Basu, ed., Pergamon, Toronto, 153 (1986).

Kobro, H., and C. Brereton, "Control and Fuel Flexibility of Circulating Fluidized Beds," *Circulating Fluidized Bed Technology*, P. Basu, ed., Pergamon, Toronto, 263 (1986).

Legros, R., C. M. H. Brereton, C. J. Lim, H. Li, J. R. Grace, and E. J. Anthony, "Combustion Characteristics of Different Fuels in a Pilot Scale Circulating Fluidized Bed Combustor," *Proc. Int. Conf. on Fluidized Bed Combustion*, 661 (1989).

Rhodes, M. J., P. Laussmann, F. Villain, and D. Geldart, "Measurement of Radial and Axial Solids Flux Variations in the Riser of a Circulating Fluidized Bed," *Circulating Fluidized Bed Technology: II*, P. Basu and J. F. Large, eds., Pergamon, Toronto, 155 (1988).

Sleicher, C. A., and M. W. Rouse, "A Convenient Correlation for Heat Transfer to Constant and Variable Property Fluids in Turbulent Pipe Flow," *Int. J. Heat Mass Transf.*, **18**, 677 (1975).

Wu, R. L., C. J. Lim, J. Chaouki, and J. R. Grace, "Heat Transfer from a Circulating Fluidized Bed to Membrane Waterwall Surfaces," *AIChE J.*, **33**, 1888 (1987).

Wu, R. L., C. J. Lim, and J. R. Grace, "The Measurement of Instantaneous Local Heat Transfer Coefficients in a Circulating Fluidized Bed," *Can. J. Chem. Eng.*, **67**, 301 (1989).

Manuscript received Jan. 20, 1989, and revision received June 12, 1989.